VOL. 13, NO. 3, FEBRUARY 2018 ISSN 1819-6608
ARPN Journal of Engineering and Applied Sciences

www.arpnjournals.com

NUMERICAL AND EXPERIMENTAL ANALYSES OF THE FLOW AROUND A ROTATING CIRCULAR CYLINDER AT SUBCRITICAL REGIME OF REYNOLDS NUMBER USING K-E AND K-Ω-SST TURBULENT MODELS

A. M. Mgaidi, A. S. Mohd Rafie, K. A. Ahmad, R. Zahari, M. F. Abdul Hamid and O. F. Marzuki
Aerospace Department, Faculty of Engineering, University Putra of Malaysia UPM Serdang, Selangor, Malaysia
E-Mail: mgaidi67@yahoo.com

ABSTRACT

An experimental investigation was conducted of a rotating circular cylinder immersed in a free-stream flow. The study was motivated by some apparent discrepancies between experimental and numerical studies of the fluid flow, and the general lack of experimental data, particularly in the subcritical Reynolds number regime. Of interest was the direction and origin of the lift force generated on the cylinder, which has been the subject of contradictory results in the literature, and for which measurements have rarely been reported. The circular cylinder was tested at 3 different free stream speeds 11, 13, and 15 m /s. The dimensionless speed ratio and Reynolds number (Re) also ranged from λ = 0.6 - 1.1, and 1.50E05 - 2.14E05, respectively. Verification of the experimental was achieved through using of computational fluid dynamics (CFD) code ANSYS FLUENT15 to simulate a two-dimensional flow of a viscous incompressible fluid past a rotating cylinder subject to a circular motion. Indeed, grid independency test (GIT) as well as the effect of domain size, have been conducted and a suitable agreement was found based on comparison of the CFD and experimental fluid dynamics (EFD) results, where a good agreement with experimental data in global quantities is predicted through generating of a fine mesh enhanced with choosing of y+ value less than 1. In the next step, the attention has been focused on comparing between the simulation results of k-ε, and k-ω -SST viscous models, to determine the most compatible model in using CFD code with the EFD results in certain mentioned condition. Generally, simulation results of each of mentioned two equations turbulent models show similar patterns as compared to EFD. A comparison of the results showed that, the margin of error in lift force coefficient was arranged from 39 - 60 % and 10 - 14% for k-ε, and k-ω -SST, respectively, which surprises the shear stress transport turbulent model as more compatible viscous model. The correspondence is seen to be excellent for analyzing the characteristic of fluid flow around the rotating objects in subcritical regime of Re.

Keywords: rotating circular cylinder, two equations turbulent models, lift force coefficient.

INTRODUCTION

The intent of this paper is to show the development and advantages, as well as disadvantages, of using computational fluid dynamics as a validation tool for existing wind tunnel experimental data of a 2D rotating circular cylinder at subcritical regime of Re. The motivation behind this validation is to develop grid generating and solving techniques that will be applied to future CFD analysis of other more complex rotating configurations at mentioned regime of Re For example, for computing the Lift force generated on spinning cylinders in Magnus rotor.

Despite the simplicity of the geometrical shape of circular cylinder, the various regimes in the flow around this object with increasing Reynolds number make numerical simulations of this flow more complex. Turbulent flow type around a circular cylinder is of great interest for understanding fundamental fluid mechanics problems. This flow type involves extremely complex physical phenomena such as flow separation due to the adverse pressure gradient, transition to turbulence and the shedding of vortices due to the interaction between both separated shear-layers [1]. According to Roshko[2], depending on the characteristics of the flow turbulent flow can be classified into four different regimes: subcritical, critical, super-critical and trans-critical, where subcritical regime is meanly limited in range of " 〖1 ×10〗 ^03≤Re ≤2 × 〖10〗 ^05". Both experimental [3-6] and numerical studies of a rotating cylinder immersed in fluid flow had been conducted before. The earliest theoretical studies concerning the steady flow were carried out by Wood [7], Moore [8] and Glauert [9, 10]. Their studies indicate that for high enough speed ratio (α), where α is defined as the ratio between the cylinder's circumferential speed velocity to the free-stream velocity, it is possible to obtain steady flows with no vortex shedding at both low and high Re. More recently, steady flows over a spinning cylinder had been investigated numerically by Tang and Ingham [11, 12] at Re = 60, 100 and α ≤0.5. On the other hand, steady-state limit of the solution of the time-dependent Navier-Stokes equations together with a verification obtained from the steady state equations had also been obtained using numerical methods by Badr *et al.* [13] for the same Re and α. The unsteady flow around a circular cylinder which starts translating and rotating impulsively from rest in a viscous fluid was investigated by Badr and Dennis [14] and Badr *et al.* [15] both theoretically and experimentally in the range of (〖1.0 ×10〗 ^03≤Re ≤2.0 × 〖10〗 ^04) and (0.5 < α < 3.0) However these investigations were based on the full Navier-Stokes equations of motion. These calculation procedures show that the numerical instabilities will give great difficulties in obtaining convergent results at higher Reynolds

numbers [11]. Steady-state numerical solutions have only been obtained for low and intermediate Reynolds numbers.

In addition to promote of research studies that aiming to verify the results of rotary objects immersed in fluid flow at subcritical Reynolds number, this study includes comparing of simulation results of 2 different viscous models at the same boundary and operating conditions that includes too, where reasonable results from two-dimensional investigation can save much more resources and achieve the performance in comparing with expensive three- dimensional simulation [14].

2. DESIGN PHASE

Geometrical dimensions of the spinning cylinder define the major element to be design in this study. A detail parameter of the cylinder is to be obtained; the main constraint in this study will be the size of the subsonic open loop wind Tunnel in Aerodynamic lab, UPM. The design parameter will be set as below as to cater to the available resource in UPM.

2.1 Specifications of the configuration and governing equations

Let us consider the incompressible unsteady airflow past a circular cylinder of diameter " D = 0.08 m" rotating with an angular velocity (Ω)of "Ω<3100rpm" in the anti-clockwise direction, as shown schematically in Fig. (1). since it is not possible to simulate numerically truly an unconfined flow, it is customary to introduce an artificial domain in the form of a box as shown schematically. Following the previous studies [6], the cylinder is placed at the center of a square domain. The flow phenomenon is described by the continuity and momentum equations written in their compact forms as follows:

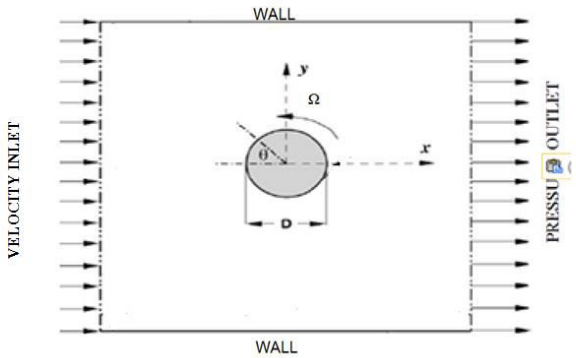

Figure-1. Schematic representation of the physical model.

2.2 Verification of wind tunnel measurements

The force measurements on a rotating cylinder are performed in the 1m x 1m low speed open loop wind tunnel at the Aerodynamic laboratory of Aerospace Engineering Department, UPM. A strut is used to amount the model on the external balance platform. The tests were conducted for free stream velocity of 11, 13 and 15m/s, respectively. For the higher free-stream velocity beyond 15m/s wind tunnel vibrates tremendously and hence it was decided not to continue the experiments beyond this free-stream velocity. Wind tunnel calibration was performed before conducting the experiment to obtain the operating conditions. For this study, the calibration between dynamic pressure and the free-stream velocity with varying frequency of the wind tunnel power supply was performed, this is derived the relationship between the free stream velocity and the frequency. Table-1 represents the data of wind Tunnel calibration.

Table-1. Wind tunnel calibrated data.

Frequency (Hz)	Dynamic Pressure (kpa.)		Calibrated Velocity (m/s)
	Calibrated	Calculated	
0	0.000	0.000	0.000
5	0.006	0.006	3.230
10	0.040	0.040	8.340
15	0.104	0.102	13.448
20	0.196	0.190	18.462
25	0.314	0.306	23.368
30	0.464	0.452	28.406
35	0.642	0.619	33.414
40	0.880	0.836	39.120

The cylinder was properly installed in the wind tunnel test section. The ambient pressure, temperature and humidity were recorded using barometer, thermometer and hygrometer respectively for the evolution of air density in the laboratory environments. The operating conditions are obtained thru the pressure calibration done during wind tunnel testing and the same conditions will be applied in the CFD simulation. Table-2 represents the main parameters of the operating condition.

Table-2. Main parameters of the operating condition.

Atmospheric Pressure (P)	1.01×10^5 N/m^2
Temperature (T)	306.15K°
Air Density (ρ)	1.1539kg/m^3
Universal Gas Constant	289
Air viscosity	1.872×10^{-5}

2.3 Turbulence modelling approach

2.3.1 Standard k-ε viscous model

It is one of two- equation turbulent model that expresses the turbulent viscosity in terms of kinetic energy" k", and its dissipation rate" ε". [18]

The following two transport partial differential equations are solved for the values of mentioned two terms as:

$$\rho u\frac{\partial k}{\partial x}+\rho v\frac{\partial k}{\partial y}+\rho\frac{\partial k}{\partial t}=\frac{\partial}{\partial x}\left\{\left(\frac{v_t}{\sigma_k}+v\right)\frac{\partial k}{\partial x}\right\}+\frac{\partial}{\partial y}\left\{\left(\frac{v_t}{\sigma_k}+v\right)\frac{\partial k}{\partial y}\right\}+v_tG-\rho\epsilon \quad (1)$$

$$\rho u\frac{\partial \varepsilon}{\partial x}+\rho v\frac{\partial \varepsilon}{\partial y}+\rho\frac{\partial \varepsilon}{\partial t}=\frac{\partial}{\partial x}\left\{\left(\frac{v_t}{\sigma_\varepsilon}+v\right)\frac{\partial \varepsilon}{\partial x}\right\}+\frac{\partial}{\partial y}\left\{\left(\frac{v_t}{\sigma_\varepsilon}+v\right)\frac{\partial \varepsilon}{\partial y}\right\}+C_1v_t\frac{\varepsilon}{k}G-C_2\rho\frac{\varepsilon^2}{k} \quad (2)$$

Where G symbolizes the generation of turbulent kinetic energy, is defined through:

$$G=2\left\{\left(\frac{\partial u}{\partial x}\right)^2+\left(\frac{\partial v}{\partial x}\right)^2\right\}+\left(\frac{\partial u}{\partial y}+\frac{\partial v}{\partial x}\right)^2 \quad (3)$$

2.3.2 Shear stress transport (SST) turbulent model

This another two- equation turbulent model was presented by Wilcox [20]. SST model is capable of showing very good prediction of the turbulence in adverse pressure gradients and separating flow. On the other hand, the shear stress transport (SST) formulation is formed by combining k–ω and k–ε models. This structure helps SST method switch to the k– ε model to avoids k– ω problem in inlet free-stream turbulence properties and uses the k– ω formulation in the inner parts of the boundary layer. Two mathematical formulas, including k and x equations, have been proposed in SST methods as below:

$$\frac{\delta}{\delta_t}(\rho k)+\frac{\delta}{\delta X_i}(\rho k u_i)=\frac{\delta}{\delta X_j}\left(\Gamma_k\frac{\delta k}{\delta X_j}\right)+G_k-Y_k+S_k \quad (4)$$

$$\frac{\delta}{\delta_t}(\rho \omega)+\frac{\delta}{\delta X_i}(\rho \omega u_i)=\frac{\delta}{\delta X_j}\left(\Gamma_\omega\frac{\delta \omega}{\delta X_j}\right)+G_\omega-Y_\omega+S_\omega \quad (5)$$

where Γk and Γω express the active diffusivity of k and ω, as well Sk and Sω that are user-defined source terms. In addition, Gk and Gω show the turbulence kinetic energy generation due to mean velocity gradients and ω, Yk and Yω also mean the dissipation of k and ω due to turbulence.

2.4 Key performance parameters

Performance of the rotating cylinder can be altered based on the various tip-speed ratios which are abbreviated as the λ.

$$\lambda=\frac{\Omega r}{U} \quad (6)$$

Tip-speed ratio (λ) of this study varies between 0.6 and 1.1 for the rotating speed velocity (Ω) 2100 RPM to 3080 RPM and wind speed 11, 13 and 15 m/s.

Additionally, Reynolds number can be obtained as follow:

$$Re=\frac{U_T L_{REF}}{\nu} \quad (7)$$

where ν represents the air kinematic viscosity at 306.15◦K, LREF is the half of the circumference of a circle, and UT is the total velocity which can be defined in the following equation:

$$U_T=U+\left(\Omega*\frac{2\Pi}{60}*\frac{D}{2}\right) \quad (8)$$

2.5 Grid generation

Before the governing equations for mass, momentum, and energy can be solved an appropriate mesh will be generated to discretize the flow domain of the model. To more accurately match the experimental conditions, the simulation is performed with the presence of wind tunnel walls as opposed to free air to capture wall effects.

2.5.1 Study of mesh impact on flow field

In order to study the influence of the mesh on the lift force output results, grid independency test (GIT) was carried out in this study and eight types of mesh were conducted.

As can be seen in Figure-2, specifically around the circular cylinder, meshes are highly denser and the y+ (wall) value is less than 1 to capture the complex flow structure with lower expected error.

2.5.2 Domain size location study

The domain size was studied to scrutinize the wake development around the spinning cylinder to avoid the blockage phenomenon on the CFD simulation. Findings of this study show that the distance of the walls (height and length of domain) can significantly affect the performance prediction of the rotating cylinder. This impact is also mentioned by other researchers [16]. Overall, 20 simulations were carried out for a circular cylinder of D diameter places at the Centre of a square domain where the length of the domain edges select to determine its dimensions relative to the cylinder diameter, outputs are illustrated in Figure-3.

As can be seen in Figure-3, the square domain edges length of less than 24D makes the blockage effect in CFD simulation and leads to inaccurate prediction of the generated lift force on the rotating cylinder. There is a very small amount of error percentage (1%) between 24D, 32D and 40D, so 24D which has a very good agreement with experimental results is selected as the most optimum size taking the simulation time into account.

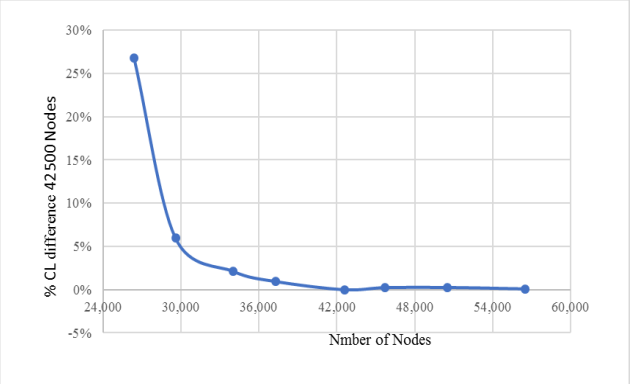

Figure-2. GIT simulation (at λ = 1.085 and V = 11 m/s).

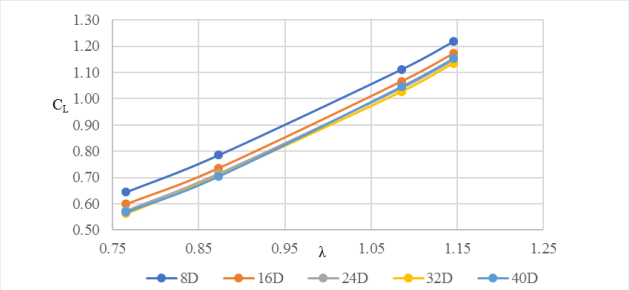

Figure-3. Variation of the lift force coefficient with different domain size.

The meshing of the model was divided in to 2 zones, the inner zone, which is a 3D x 3D block around the circular cylinder, and the outer zone, which is the zone away from the rotating object. For the inner zone, near the surface of the cylinder a consecutive boundary layers carried out throughout, to ensure that value of y+<1 through high of the nearest cells to the cylinder. As for the outer zone, it divided to 4 faces through 4 interior edges to achieve a good structured mesh to accurately model the viscous forces. Figure-4 shows cut plane of mesh in domain and cylinder and Table-3 presents some of main mesh parameters.

Table-3. Some of main mesh parameters..

Details of Mesh	
Relevance center	Fine
Smoothing	High
Element Minimum Size	0.52852mm
Maximum Face Size	52.852mm
Growth Rate	1.2
Details of Inflation	
Transition Ratio	0.272
Option	Smooth Transition
Maximum layers	14
Growth rate	1.05

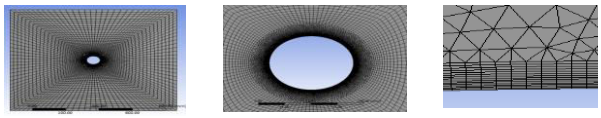

Figure-4. Computational domain and the implemented grid for the numerical simulations.

3. SOLVER SETTINGS AND BOUNDARY CONDITIONS

Once a good quality mesh has been generated throughout the entire domain, the mesh file is then loaded into the CFD solver, Fluent Ansys15. Before the governing equations can be solved, the appropriate settings must first be enabled throughout Fluent's interface and the correct boundary conditions must be specified to accurately match the conditions in which the experimental evaluations were performed. Table-4 shows a list of constant solver settings that have been considered to investigate the numerical simulations.

Table-4. Solver settings that have been considered to investigate the numerical simulations.

ANSYS Fluent 15 Solver Settings	
Standard k-ω, and k-ω-SST	
Type: Pressure-Based , Time: Transient	
Ideal-gas Law	
Method:	Pressure – velocity coupling
Residual error	1.0 E-06
Scheme:	Coupled
Spatial Discretization	
Gradient	Green- Gauss Node Based
Pressure	PRESTO
Momentum	QUICK
Turbulent KE	QUICK
Specific Dissipation rate	QUICK
Time step	1_ rotation per time step
Free stream Conditions	
Pressure	101.325kpa
Velocity	11, 13, and 15 m/s
Temperature	306.15k°

3.1 Numerical simulation

Numerical simulations presented in this study, are integrated in the framework of the commercial fluid dynamics package Fluent Ansys15. The elliptic partial differential equations are solved by the finite-volume method. The system of the algebraic equations is solved in a coupled iterative manner. Therefore, the velocity and the pressure fields are updated together. This is a coupled pressure-velocity procedure, which is very efficient and converges faster than the classical segregated approaches for well-behaved problems [21]. The fully implicit coupling is achieved through an implicit discretization of the pressure gradient terms in the momentum equations, and an implicit discretization of the mass flux

4. RESULTS AND DISCUSSIONS

4.1 Experiment tests

Tests were conducted on the rotating cylinder model. Wind tunnel measurements using the real model were done at Reynolds numbers 5.42×10^4, 6.41×10^4 and 7.40×10^4. The rotating cylinder is mounted onto the six component external balance, which connected to the computer device and converts the lift force into digital values thru a data acquisition. Figure-5 is prepared through the above data to show the change in pattern of lift force

with the change of rotational speed of the cylinder. It is seen that there is an increasing in a measured lift force with an increased in rotational rate of a spinning cylinder at constant free-stream's speed. The increasing in the lift force has been also with the increase in Reynolds number in the mentioned regime.

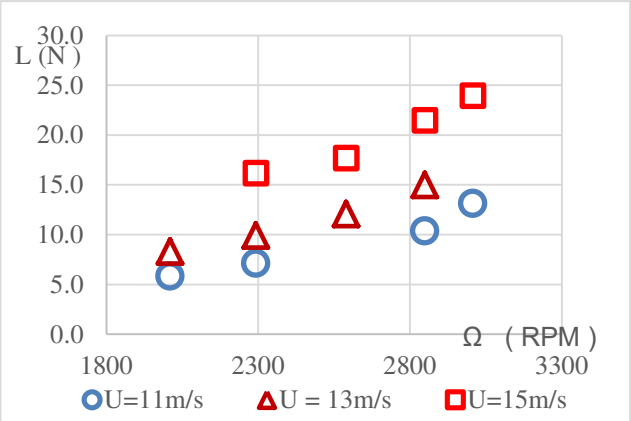

Figure-5. Experimental results of lift force versus rotational speed.

4.1.1 Calculation of lift coefficient

Lift Coefficient is defined as [14]

$$c_L = \frac{L}{0.5\rho U_\infty^2 S} \quad (9)$$

For the three mentioned values of free-stream velocity at a range of spinning rate corresponding Lift force coefficient are given in Table-5.

Table-5. Calculated experimental lift force coefficient.

Free- stream Velocity	Wind Tunnel Experimental Lift Force Coefficient " C_L "					
m/s	Ω=0 rpm	Ω=2010 rpm	Ω=2293 rpm	Ω=2590 rpm	Ω=2850 rpm	Ω=3008 rpr
11	0.0000	0.6637	0.8099		1.1798	1.4955
13	0.0000	0.6773	0.9104	0.9851	1.2230	
15	0.0000		0.9920	1.0845	1.3165	1.4683

4.2 Numerical simulation

As noted earlier, the present flow analysis is governed by three dimensionless parameters, namely, CL, Re and λ_c and the principal aim of the present study is to develop this functional relationship. However, prior to embarking upon the presentation of new results, it is useful to demonstrate the adequacy of the numerical computations which will also help ascertain the accuracy of the new results reported herein. Y. M. Shim *et al* [14] pointed to a good agreement with experimental data in global quantities, when they compared with their 2-D numerical results of analyzing air flow around rotating cylinder in sub- critical Reynolds number.

Figures 6, 7, and 8 represent the pattern of changing in CL versus λ, according to both of EFD and CFD results of each of k-ε, and k-ω- SST models, in order to choose the most appropriate and achieve the verification. The better performance of two-equation model can be reassured. It is observed that each of mentioned two equations turbulent models show similar patterns as compared to experimental results. Besides that, it may be said from both of numerical and experimental results that CL tend to rise with increasing of λ in the chosen range. On other hand, it is clearly seen that the values of lift force coefficient CL obtained from k-ε is greater than that obtained from k-ω -SST model. It is probably due to the fact that the stagnation point obtained from k-ε model is closer to the cylinder compared to the stagnation point obtained from other one. It is evident that the values of CL predicted with k-ω- SST models is in better agreement with the experimental data than the results of obtained from k-ε.

As can be seen Figures 6, 7, and 8, the comparison shows a very good agreement between 2D simulation and EFD results. In the range of $0.6 < \lambda < 1.2$, decrements of the CL prediction k-ω -SST is less than 14%. Clearly, the lowest error of the prediction CL was (4% error) is in $\lambda = 0.723$ at " U= 15m/s ". Conversely, the worst result of 15% error, which has occurred at high spinning rate of cylinder. This inaccurate result occurred maybe because of some errors in the experimental test at high rotational speeds and using the fully turbulent model. In addition, instability mechanisms in the stationary/rotating zones may be one of the reason which lead to these differences [18]. Turkyilmazoglu [19] employed linear stability theory to obtain the stability characteristics of the incompressible boundary layers.

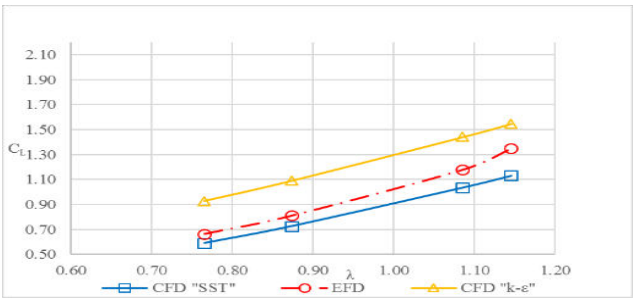

Figure-6. Comparison of the CFD and EFD data (at $0.7 < \lambda < 1.2$ and U = 11 m/s).

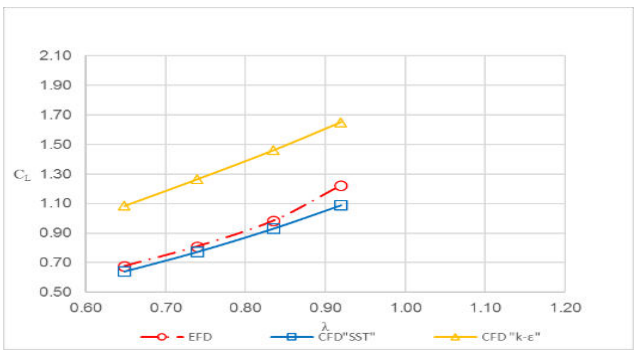

Figure-7. Comparison of the CFD and EFD data (at $0.7 < \lambda < 1.2$ and U = 13 m/s).

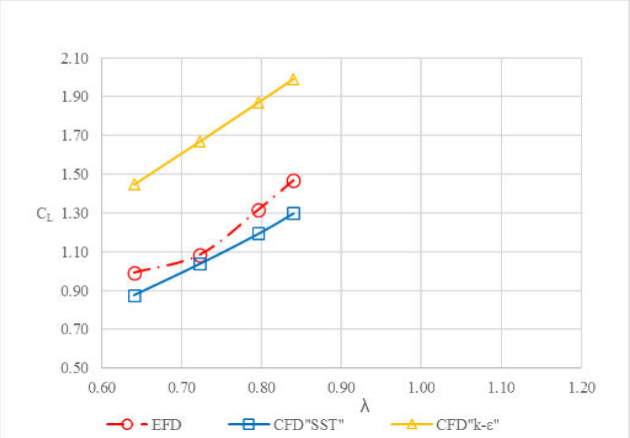

Figure-8. Comparison of the CFD and EFD data (at $0.7 < \lambda < 1.2$ and U = 15 m/s).

5. CONCLUSIONS

In this study, two-dimensional simulations have been carried out using of Fluent ANSYS15 to verify the experimental investigation that has conducted to free-stream flow over a rotating circular cylinder at subcritical regime of Reynolds number. In order to identify the most compatible viscous model to experimental results. For this work, grid dependency test was designed to determine the best quality mesh. Effects of the domain size were also investigated and the results showed that the square domain model of 24D (in Figure-3) has no effect on CL prediction on spinning cylinder. Furthermore, forty-five simulation runs are executed at a four chosen spindle rates of the cylinder using of each of chosen CFD models. From the comparisons of EFD and CFD results, it is observed that CL tend to rise with increasing of λ in the certain range. On other hand, the simulations using k-ω -SST viscous model are found generally more accurate than k-ε model. According to the results of k-ε and k-ω -SST models, maximum amount of discrepancy was reached 60%, and 14%, respectively. In conclusion, it is evident that, CL predicted from k-ω -SST model is more closed to experimental results. The correspondence is seen to be excellent for analyzing the characteristic of fluid flow around the rotating configurations in subcritical regime of Re.

Nomenclature

Symbol	Description (Unit)
CFD	Computational fluid dynamics Greek
C_L	Lift coefficient
λ	Tip speed ratio
D	Diameter of the cylinder (mm)
ε	Turbulent dissipation rate
GIT	Grid independency test
ω	Dissipation per unit turbulent kinetic energy dissipation)
EFD	Experimental fluid dynamics
Ω	Rotational speed of the cylinder (RPM)
P	Atmospheric pressure (N / m^2)
μ	Viscosity (N. s /m^2)
R	Universal gas constant
ρ	Density (kg / m^3)
Re	Reynolds number
ν	Kinematic viscosity (m^2 / s)
SST	Shear stress transport
T	Atmospheric temperature (K°)
U	Air flow speed (m/s)

REFERENCES

[1] J. H. Gerrard. 1966. The mechanics of the formation region of vortices behind bluff bodies. J. Fluid Mech. 25, 401-413.

[2] A. Roshko. 1961. Experiments on the flow past a circular cylinder at very high Reynolds number. J. Fluid Mech. 10, 345-356.

[3] W.M. Swanson. 1961. The Magnus effect: A summary of investigations to date. J. Basic Eng. 83, pp. 461-470.

[4] G.R. Ludwig. 1964. An experimental investigation of laminar separation from a moving wall. AIAA Paper 64-6.

[5] M. Coutanceau and C. Menard. Influence of rotation on the near-wake development behind an impulsively.

[6] H. Peller. 1986. Thermo fluid dynamic experiments with a heated and rotating circular cylinder in cross flow, Part 2.1: Boundary layer profiles and location of separation points. Exp. Fluids. 4, pp. 223-231.

[7] W.W. Wood. 1957. Boundary layer whose streamlines is closed. J. Fluid Mech. 2, pp. 77-87.

[8] D.W. Moore. 1957. The flow past a rapidly rotating circular cylinder in an infinite stream. J. Fluid Mech. 2, pp. 541 550.

[9] M.B. Glauert. 1957. The flow past a rapidly rotating circular cylinder. Proc. R. Soc. Ser. A 230, pp. 108-115.

[10] M.B. Glauert. 1957. A boundary layer theorem with applications to rotating cylinders. J. Fluid Mech. 2, pp. 89-99.

[11] T. Tang and D.B. Ingham. 1991. On steady flow past a rotating circular cylinder at Reynolds numbers 60 and 100. Comput. Fluids. 19(2): 217 230.

[12] D.B. Ingham and T. Tang. 1990. A numerical investigation into the steady flow past a rotating circular cylinder at low and intermediate Reynolds numbers. J. Comput. Phys. 8%. pp. 91 107.

[13] H.M. Badr, S.C.R. Dennis and P.J.S. Young. 1989. Steady and unsteady flow past a rotating circular cylinder at low Reynolds numbers. Comput. Fluids. 17(4): 579-609.

[14] John D. Anderson, Jr. 2015. Fundamentals of aerodynamics.

[15] M. Cheng, Y.T. Chew, S.C. Luo. Discrete vortex simulation of the separated flow around a rotating circular cylinder at high Reynolds number. Department of Mechanical and Production Engineering, National University of Singapore, Singapore 0511, Singapore.

[16] Mohamed MH, Ali AM, Hafiz AA. CFD analysis for H-rotor Darrieus turbine as a low speed wind energy converter. Eng Sci Technol. Int. J 2015(0).

[17] Menter FR. 1994. Two-equation eddy-viscosity turbulence models for engineering applications. AIAA J. 32(8): 1598-605.

[18] Launder B.E and Spalding D.B. 1974. The numerical computation of turbulent flows. Computer Methods in Applied Mechanics and Engineering. 3: 269-289.

[19] Turkyilmazoglu M. 2003. Instability of the flow in the vicinity of trailing edge of a class of thin aerofoils. Comput Fluids. 32(3): 353-71.

[20] Wilcox D.C. 1988. Reassessment of the scale-determining equation for advanced turbulence models. American Institute of Aeronautics and Astronautics Journal. 26(11): 1299-1310.

[21] S. J. Karabelas, B.C. Koumroglou, C.D. Argyropoulos, N.C. Markatos. High Reynolds number turbulent flow past a rotating cylinder. Computational Fluid Dynamics Unit, School of Chemical Engineering, National Technical University of Athens, 9 Iroon Polytechniou Str., Zografou Campus, GR-15780 Athens, Greece.